九州大学学術情報リポジトリ
Kyushu University Institutional Repository

Numerical study on the Effect of Rectangular and Triangular Counter-Rotating Vortex Generators on the H-Rotor Wind Turbine Performance

Yaningsih, Indri
Department of Mechanical Engineering, Faculty of Engineering, Universitas Sebelas Maret

Dominicus Danardono Dwi Prija Tjahjana
Department of Mechanical Engineering, Faculty of Engineering, Universitas Sebelas Maret

Eko Prasetya Budiana
Department of Mechanical Engineering, Faculty of Engineering, Universitas Sebelas Maret

Muqoffa, Mohamad
Architecture Department, Faculty of Engineering, Universitas Sebelas Maret

他

https://doi.org/10.5109/6781073

出版情報：Evergreen. 10 (1), pp.230-241, 2023-03. Interdisciplinary Graduate School of Engineering Sciences, Kyushu University, Japan
バージョン：
権利関係：Creative Commons Attribution-NonCommercial 4.0 International

KYUSHU UNIVERSITY

Numerical study on the Effect of Rectangular and Triangular Counter-Rotating Vortex Generators on the H-Rotor Wind Turbine Performance

Indri Yaningsih[1,*],Dominicus Danardono Dwi Prija Tjahjana[1,*], Eko Prasetya Budiana[1], Mohamad Muqoffa[2], Zainal Arifin[1], Suyitno[1], Koji Enoki[3], Takahiko Miyazaki[4]

[1]Department of Mechanical Engineering, Faculty of Engineering, Universitas Sebelas Maret, Jl. Ir. Sutami 36 A, Surakarta 57126, Indonesia

[2]Architecture Department, Faculty of Engineering, Universitas Sebelas Maret, Jl. Ir. Sutami 36 A, Surakarta 57126, Indonesia

[3]Department of Mechanical and Intelligent System Engineering, The University of Electro-Communication, 1-5-1, Chofugaoka, Chofu-shi, Tokyo 182-8585, Japan

[4]Thermal Energy Conversion System Laboratory, Interdisciplinary Graduate School of Engineering Sciences, Kyushu University, 6-1 Kasuga-koen, Kasuga-shi, Fukuoka 816-8580, Japan

*Author to whom correspondence should be addressed:
E-mail: indriyaningsih@staff.uns.ac.id (I.Y), ddanardono@staff.uns.ac.id (D.D.D.P.T)

(Received December 8, 2022; Revised March 3, 2023; accepted March 4, 2023).

Abstract: Vortex generators (VGs) in the form of small fins are attached to the blade of the H-rotor wind turbine to improve the performance. Many studies provide the utilization VGs both experimentally and numerically. However, the investigation of the full scale of counter-rotating VGs in rotor blades is still rarely found. In the current study, two shapes of VGs were investigated to evaluate wind turbine performance. VGs in rectangular and triangular shapes were attached under the identical blade geometry of 375 mm of chord length and the blade attachment of 30% from the chord length. VGs have a similar height and length of 6.5 mm and 13 mm, respectively. The turbine was constructed with three blades that rotate under 1,650 mm of the rotor diameter and 1,000 mm of rotor height. The chordwise position (x/c) of the VGs was at 10%, 15%, 20%, and 25%. The computational fluid dynamics with the unsteady Reynolds Average Navier Stokes (URANS) model were employed. We found that VGs behave in different performances. The rectangular VGs had the maximum power coefficient (Cp) value at the x/c of 20%, while the triangular VGs had the maximum Cp value at the x/c of 25%. However, both VGs show the maximum Cp in the value of 0.467 with a 1.5 Tip Speed Ratio. To evaluate the performance improvement, the blade with VGs was compared with the blade without VGs. It was found that using the VGs improved the performance of the wind turbine by around 45.68% and 47.24%, respectively, for triangular and rectangular shapes. The flow field characteristics in terms of turbulent kinetic energy and flow velocity were also presented in this study to gain a better understanding of how the VGs work. The result revealed that the presence of the VGs significantly improves the performance of the turbine.

Keywords: blade; rotor; coefficient of performance; vortex generator; wind turbine

1. Introduction

The increase in energy demand will be a crucial issue for the next few years. In an attempt to maintain the energy supply, the development of alternative energy sources concerning renewable energy is now growing increasingly. The employment of renewable energy sources such as solar[1,2], wave[3,4], geothermal[5,6], tidal[7,8], and wind[9,10] have been widely investigated to evaluate their potency. The renewable energy source can undoubtedly provide the energy supply though it still requires a system improvement to achieve high performance. Among the renewable energy sources, wind energy is one of the most common types of renewable energy, contributing to the fastest-growing sources of electricity[11]. The wind is clean and efficient to be used in land space, yet the nature of intermittent sources makes wind energy incapable of

providing constant energy. The performance of the wind turbine relies on the weather. When the wind speed is low, the rotor will not spin, decreasing the wind turbine's performance. Slow-moving air towards the blade of the wind turbine during the low wind speed, generally less than 4.4 m/s, only provides a small amount of torque to rotate the blades. The power density for a wind speed of fewer than 4.4 m/s will be no more than 100 W/m^2. Besides, the turbine's rotor will only spin when the lift's force is stronger than the drag.

The targeted plan of wind energy technologies is to improve their performance. For the last few decades, the vertical axis wind turbine has attracted more attention in research activities regarding performance improvement. Modifying the turbine blade and rotor is one of the keys to achieving good aerodynamic performance and the operation of the wind turbine[12,13,14,15]. The aerodynamics of wind turbines mainly depends on the flow characteristics. Delaying the flow separation[16,17], generating stream-wise vortices[17,18], and controlling stalls [19,20] are the mechanism of aerodynamics performance improvement. Some mechanisms can be achieved using the vortex generators (VGs) attached to the blade surface. Jiang et al.[21] used VGs on rotating wind turbine blades. The VGs increased the lift coefficient by 4.4.% and 6%, respectively, at 10 m/s and 13 m/s of rotational speed. The VGs could delay the flow separation, thus improving the lift coefficients. The combination of VGs and leading-edge roughness (LER) was studied by Chengyong et al.[22]. Controlling the dynamic stall was their goal to improve the aerodynamic performance. They found that the presence of VGs could delay the dynamic stall, reduce the aerodynamic hysteresis, and suppress the separated flow. At the same time, the LER contributes to increasing the turbulent kinetic energy (TKE). Mereu et al.[23] investigated the VGs applied in the thick blade to model the stall behavior. The VGs successfully delay the stall on the high attack angle, leading to increased blade performance. Not only delay, but the VGs also might suppress the dynamic stall depending on the configuration of the VGs[24]. The height and mounting position will be the important factor investigated by Tavernier[24].

The selection of VGs geometrics parameters, including position, orientation, layout, shape, and height, will be mandatory when designing the wind turbine blade. Different position of VGs in rotational blades was studied by Zhu et al.[25]. The skewed layout of VGs effectively reduces the separation bubble. VGs also increased the maximum lift coefficient by 60%. Installing VGs at different chordwise positions would also improve the aerodynamics performance. The chordwise position is important in developing the blade configuration, mainly when applied to the rotational turbine. Unexpected stalls might occur when the location of VGs too far downstream. Zhang et al.[26] suggest that the VGs should be placed at x/c > 20% under the small attack angle to avoid the lift coefficient decrease. Similar results were also found by Lengani et al. [27] that x/c = 20% was the most effective position for delaying the stall, particularly for counter-rotating VGs. The VGs orientation can be in co-rotating and counter-rotating, which will have different behavior towards the flow. A co-rotating direction develops longitudinal vortices, which drive the fluid momentum upward for the low momentum and downward for the high momentum. Conversely, the counter-rotating VGs detached the momentum transport. Supposedly, counter-rotating would be more effective than co-counter rotating [28]. Hansen et al. [29] also found that counter-rotating performs better than co-rotating.

Above specific critical geometry, the layout for single or double-row vortex generators would also be interesting to be investigated. A single-row and double-row of VGs take their own part in aerodynamics performance. As mentioned by Zhu et al. [30], the single-row VGs contribute more to flow-reattachment while the double-row VGs promote the flow near-wall, weakening the pressure gradient [30]. A single-row and double-row VGs can consist of rectangular, triangular, circular, or even trapezoidal VGs. The different shapes own unidentical longitudinal vortices strengths. As a result, it is revealed a different typical flow separation effect of VGs[28]. Effective longitudinal vortices and durable turbulence flow give the flow around the VGs more resistance to flow separation in unfavorable pressure gradients affecting the production cost. Therefore, the accurate selection and application of VGs can save on production costs, producing more competitive wind energy technology with power production improvement.

Corresponding to previous work, we propose a novel blade design by attaching the triangular and rectangular VGs to the blade surface. To the best of our knowledge, the very limited study provides a full-scale numerical study for rotating rotors containing blades with VGs, particularly on H-rotor turbines. The combination of chordwise positions (x/c) is provided to investigate the aerodynamics characteristics and wind turbine performance in terms of power coefficient (Cp). The torque and flow field characteristics are evaluated accordingly. The simulations of the computational fluid dynamics (CFD) with the unsteady Reynolds Average Navier Stokes (URANS) model are performed to assess the flow behavior behind the blade due to the presence of the VGs. The evaluation is conducted by comparing the turbine with and without VGs. The turbine without VGs is considered as the base line. The visualization of the turbulent kinetic energy and the flow field is provided to support the simulation results. The current research contributes to offering guidance for designing wind turbine blades.

2. Numerical Technique

The turbine blade design starts with selecting the airfoil. NACA 0015 airfoil was chosen since Mohamed et al.[31] found that NACA 0015 performed the highest power

coefficient for the H-rotor turbine. The CFD software ANSYS Fluent is used in the study to perform all the computations. The computations were conducted for the blade without VGs, the blade with rectangular VGs, and the blade with triangular VGs.

2.1 Computational Domain and Vortex Generators Geometry

The computational domain, represented by the enclosure, consists of rotating and stationary regions, as shown in Figure 1. The stationary region was designed with a length of 15D and a width of 10D, where *D* is the rotor diameter of the wind turbine.

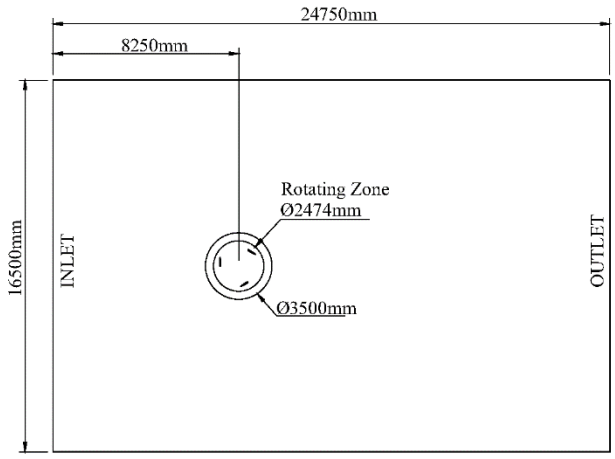

Fig. 1: Schematic of enclosure the computational domain.

The rotor diameter (*D*) used in the current study was 1,650 mm. The rotor consists of three blades which consider as the rotating zone. The blade chord length (*c*) was 375 mm. The direction of blade rotation was in a counter-rotating direction. The blades were attached to the rotor arm at 30% of the chord length. Though, in the simulation, the rotor arm and shaft were not included. The parameter design for the validation was referred to Song et al. [32]. Table 1 shows the details of the parameter design of the H-rotor turbine.

Table 1. Parameter of H-rotor turbine.

Parameters	Symbol	Value
Wind velocity (m/s)	$V\infty$	8
Blade number (-)	*N*	3
Rotor diameter (mm)	*D*	1650
Blade chord length (mm)	*c*	375
Blade attachment (mm)	-	30%c

Song et al.[32] used 2D simulation for their study. Therefore, in the validation case, the current study also conducted the validation using a 2D H-rotor wind turbine and compared the results for the evaluation. After achieving the satisfied value for the validation, less than 10%, the simulation will further investigate the performance of the wind turbine by using the 3D simulation.

To investigate the effect of the VGs on the wind turbine, the comparison of the blade with and without VGs is provided in the current study. The blade without VGs was used as the baseline. The blade height was set as 1,000 mm with a rotor diameter of 1,650 mm, as shown in Fig. 2. While the addition of the VGs into the turbine blade was shown in Fig. 3. The red box in Fig. 3 shows the VGs installment onto the wind turbine.

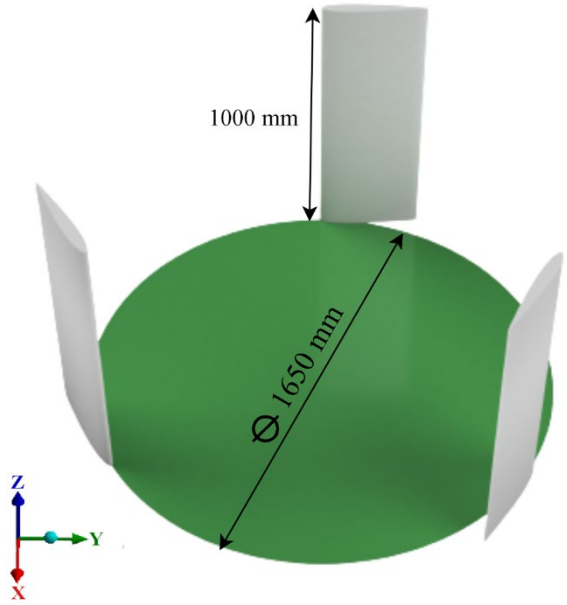

Fig. 2: Blade 3D modelling without VGs.

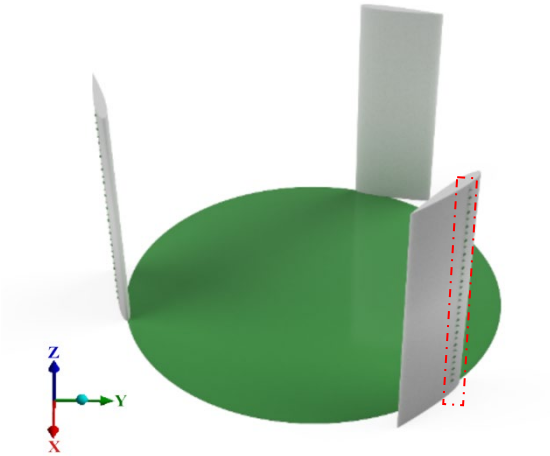

Fig. 3: Blade 3D modelling with VGs.

The VGs in the current study was modified as a triangular and rectangular shape. The height, length, and thickness for both were kept constant at 6.5 mm, 13 mm, and 1.3 mm, respectively. The details of the VGs employed in the current study can be seen in Figure 4 (a) and (b), respectively, for triangular and rectangular shapes.

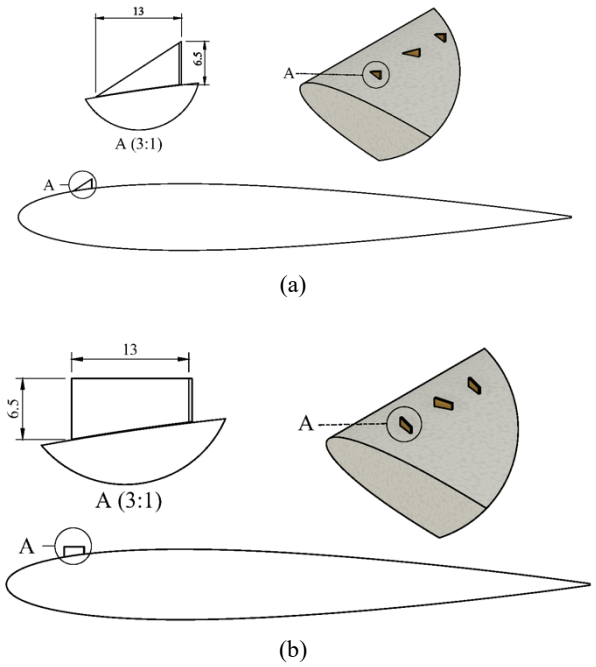

Fig. 4: (a) Triangular VGs, (b) Rectangular VGs.

Figure 5 shows the VGs arrangement on the blade surface. The VGs were arranged as a pair with a constant spanwise of 32 mm toward the incoming airflow while the angle between the VGs position and flow direction was 75°. The setting position was similar both for rectangular and triangular VGs.

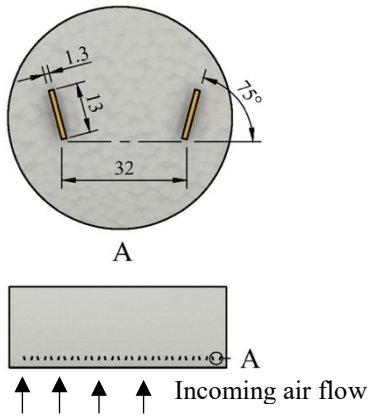

Fig. 5: The VGs arrangement on the blade surface.

The modified parameter in this study was the chordwise position (x/c). The x/c was set at 10%, 15%, 20%, and 25% for both VGs. As a consequence of x/c modification, the VGs position from the chord will be 37.5 mm, 56.25 mm, 75 mm, and 93.75 mm, respectively, for x/c of 10%, 15%, 20%, and 25%. Figure 6 depicts the position of the VGs towards the chord length.

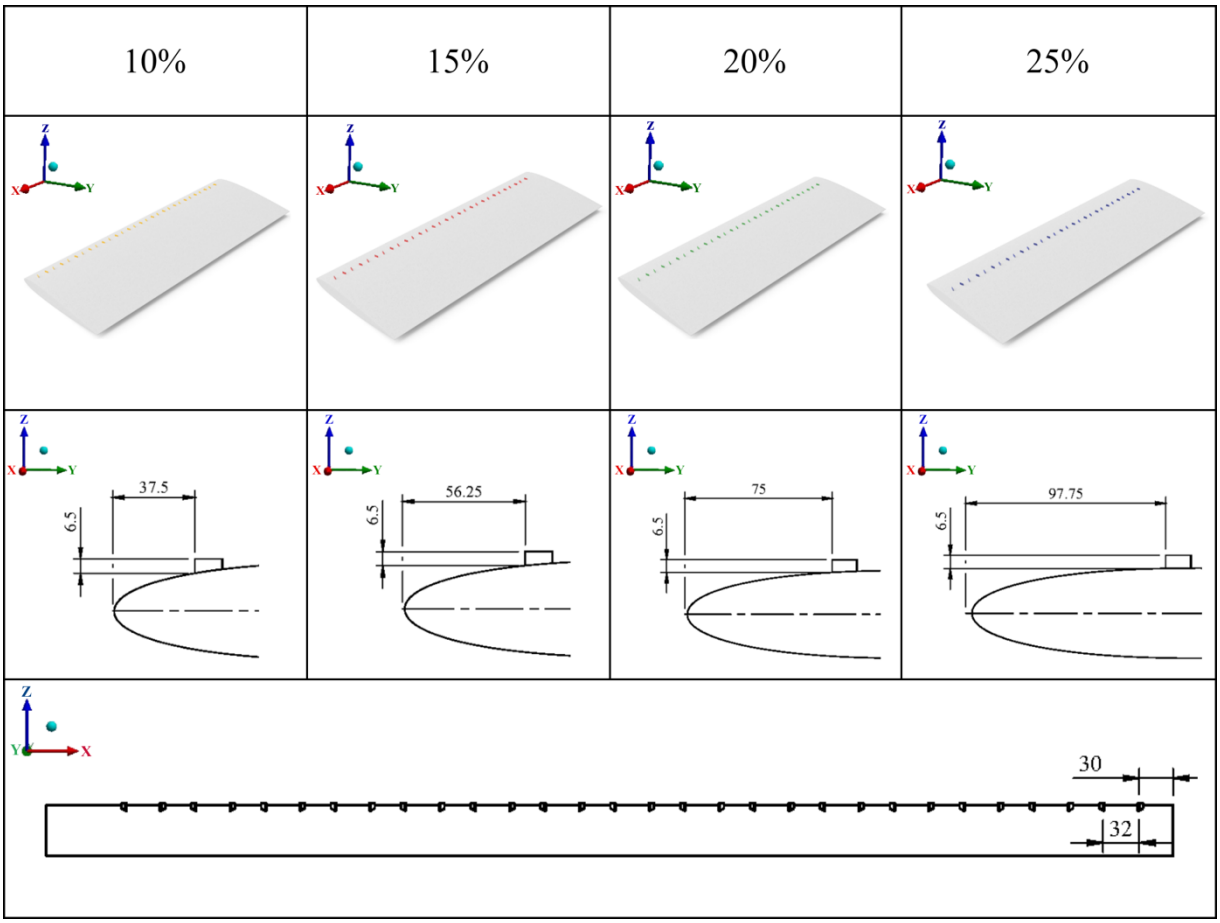

Fig. 6: The VGs position towards chord length.

2.2 Computational Fluid Dynamics Simulation

The Semi-Implicit Method for Pressure-Linked Equations (SIMPLE) was used to solve the Incompressible Unsteady Reynolds-Averaged Navier-Stokes (URANS). The flow in the current simulation was considered as an unsteady incompressible viscous flow. The governing equation for continuity and momentum is as follows[33]:

$$\frac{\partial u_j}{\partial x_j} = 0, \quad (1)$$

$$\frac{\partial u_i}{\partial t} + u_j \frac{\partial u_i}{\partial x_j} = -\frac{1}{\rho}\frac{\partial p}{\partial x_i} + \frac{\partial}{\partial x_j}\left(v \frac{\partial u_i}{\partial x_j}\right) + f_i \quad (2)$$

where t represents the time, ρ is fluid density, u is the fluid velocity, and p is the pressure. The x_i and x_j are cartesian coordinate components while f_i is the body force per unit volume.

The turbulent model was simulated using Realizable k-ε. It is referred to Song et al.[33], who compared six turbulence models for 2D unsteady models of VAWT, including the Realizable k-ε model. They found that, for rotating simulation, the Realizable k-ε model is the best option to show the rotation and curvature effect as well as give more acceptable accuracy. Besides, the Realizable k-ε model also has the ability to simulate the flow field that occurs in the modeling. The pressure, turbulent kinetic energy, and specific dissipation rate were solved using a second-order interpolation scheme. The numerical settings detail is tabulated in Table 2.

Table 2. The simulation settings.

Parameters	Value
Fluid density	1.225 kg/m^3
Fluid viscosity	1.7894 x 10^{-5} kg/m.s
Inlet boundary	Velocity inlet, 8 m/s
Outlet boundary	Pressure outlet
Latera sidesl boundary	Symmetry
Blades boundary	No-slip wall
Contact Region between rotating and stationary region boundary	Sliding grid interface
Solver type	Pressure Based
Viscous model	Realizable k-ε
Residual Error	1 x 10^{-4}

2.3 Mesh Generation

The tetrahedral meshing method was applied in the current simulation. The size meshing function of proximity and curvature mesh type has been applied to ensure the mesh quality of curvature area on the rotating domain and airfoil. To improve the mesh accuracy, the cell size was limited by 100 mm for all domains. In addition, the accuracy was also enhanced by applying body sizing with a 50 mm element size for the rotating domain where the wind turbine was applied. Not only the rotating domain but also the enclosure where the turbine rotates; the body sizing was applied with an element size of 50 mm. The generated mesh has 1,775,328 nodes and 1,695,154 elements. Figures 7 (a) and (b) show the mesh configuration of the rotating and far-field domains. The mesh is gradually refined along the region close to the blades; hence the details of the flow fields during the rotation can be captured.

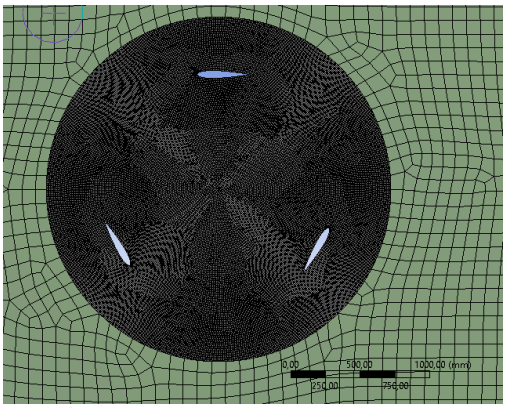

(a)

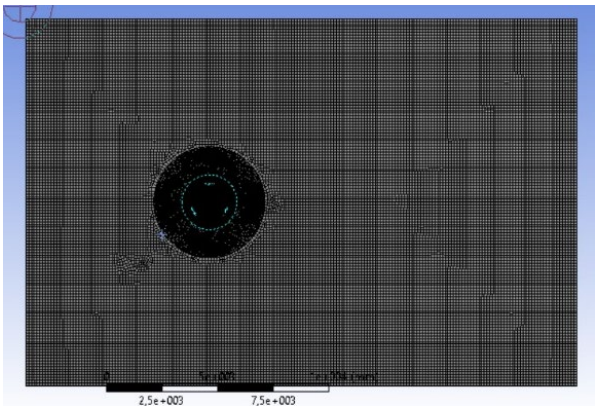

(b)

Fig. 7: The mesh configuration on the (a) rotating domain; (b) far field domain.

Figures 8 (a) and (b) show the mesh generation for single VGs and whole VGs in the 3D simulation, respectively. The tetrahedral mesh was applied for the VGs with a maximum face size of 50 mm and a minimum face size of 1 mm. The presence of the VGs revealed the increase of the mesh element by 2,865,136 with 936,230 nodes. The maximum and average skewness was found to be 0.801 and 0.196, which satisfied the mesh requirement for the tetrahedral mesh type. The maximum skewness of tetrahedral mesh should be lower than 0.95 with an average value of less than 0.33[34]. Based on the mesh evaluation, the identical mesh was applied for both VGs.

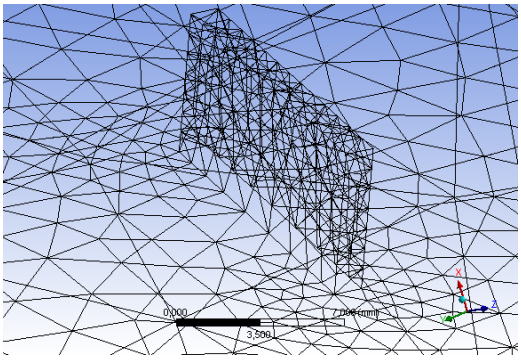

(a) Mesh for single VGs.

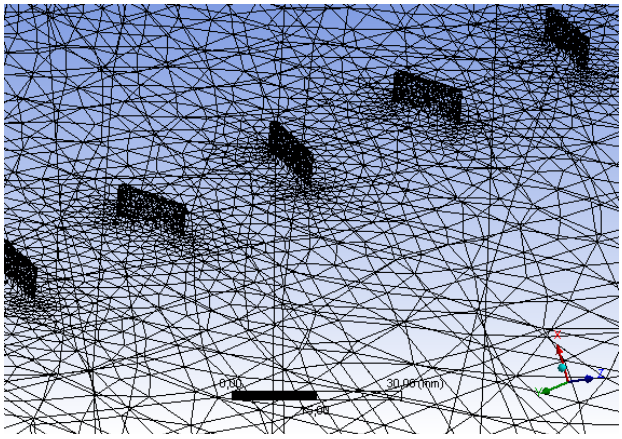

(b) Mesh for whole VGs.

Fig. 8: Mesh for (a) single VGs, (b) whole VGs.

2.4 Boundary conditions

Figure 9 depicts the boundary conditions set up for the computational domain.

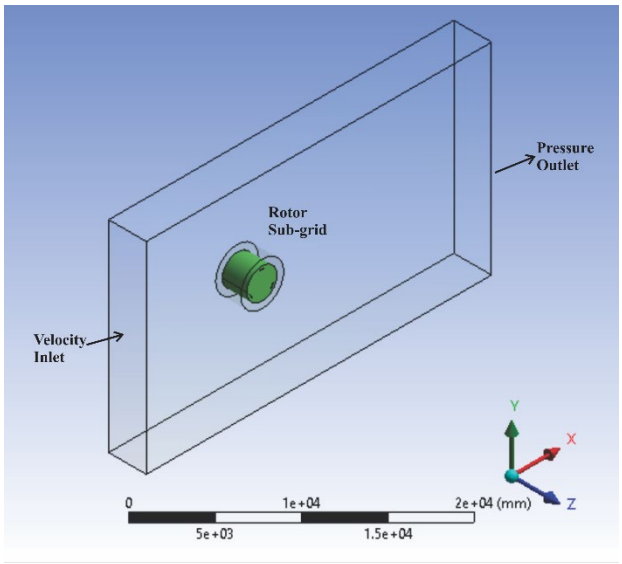

Fig. 9: Boundary condition on the 3D domain.

The simulation was a free-stream transient, pressure-based condition. The rotor sub-grid, in which a rotating domain was set at constant velocity depending on tip speed ratio (TSR). The velocity inlet was 8 m/s. The outlet was set as a pressure outlet. The upper and bottom walls were assumed as smooth walls with zero shear stress or slip walls. Near-wall treatment was applied using enhanced wall treatment to model the turbulent flow with $y+ < 5$.

The simulation process for the blade with and without VGs is conducted by changing the tip speed ratio (TSR) value. There are five variations of TSR, starting from 0.5 to 2.5 with a 0.5 increment. The simulation output is the moment coefficient (Cm) for each time step. Then the power coefficient (Cp) value can be calculated by the following equation:

$$Cp = TSR.C_{m,ave} \quad (3)$$

2.5 Validation

The validation was conducted by evaluating the current result with reference [32]. Figure 10 compares the recent result and the reference's power coefficient value (Cp). As shown, the discrepancy was relatively small. The maximum discrepancy was 15.22 % at a TSR of 2.5. It implies that the agreement of the results in terms of Cp was good at a low rotational speed. The average discrepancy was found in the value of 8.7%. It means that the model was satisfied with the reference.

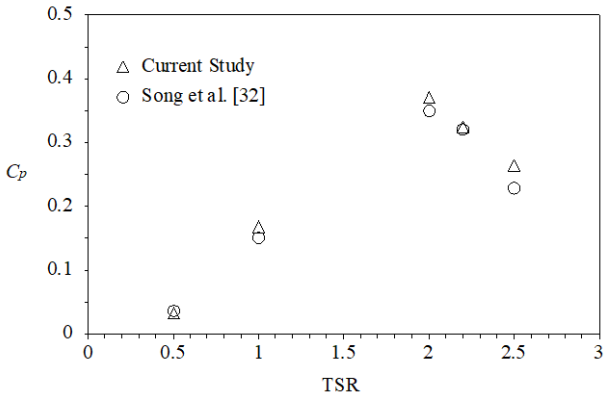

Fig. 10: Comparison of Cp value of the current study and reference [32].

3. Results and Discussion

Once the validation for the simulation is achieved, the modeling of the H-rotor wind turbine can be conducted. The simulation was conducted in the 3D modeling method. The moment coefficient (Cm) and power coefficient (Cp) are calculated to evaluate the performance. The Cm and Cp values of the rotor blade with VGs are compared with the rotor blade without VGs to assess the performance enhancement of the turbine.

3.1 The effect of Vortex Generators on Moment Coefficient (Cm)

The variation of the Cm is analyzed for azimuth angle, θ. Figure 11 shows the azimuth angle definition in the rotor plane for blades 1, 2, and 3.

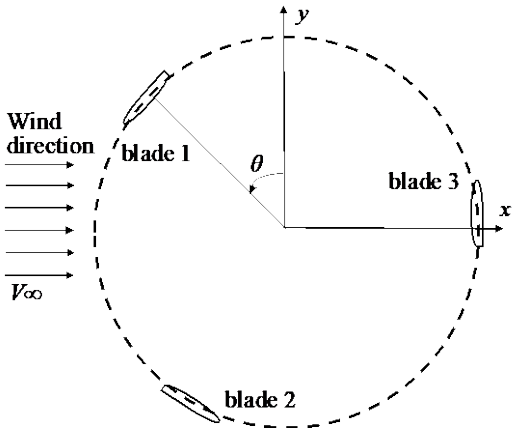

Fig. 11: Azimuth angle definition (θ).

The moment coefficient (Cm) of the rotor blade without VGs is provided in Figure 12.

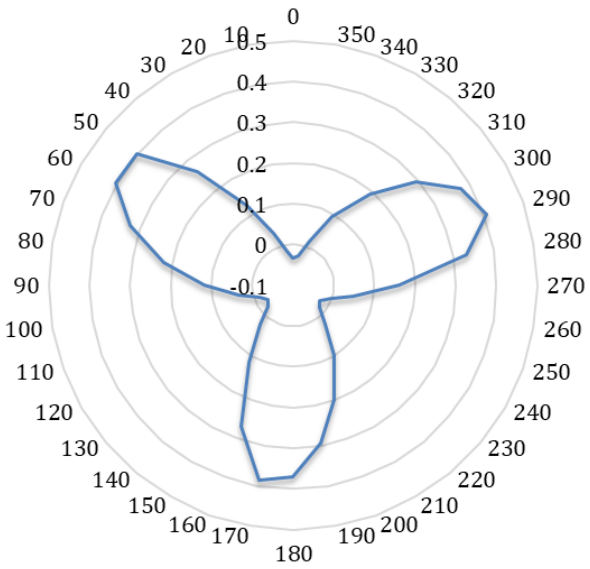

Fig. 12: Polar chart of Cm with respect to θ during one rotational period at TSR of 1 for rotor blade without VGs.

Figure 12 plots the polar chart at TSR of 1 for one rotational period; since the rotor contains three blades, the curve repeats after 120°. Figure 12 exhibits that the maximum Cm value occurs when the turbine rotates at θ of 60°, 180°, dan 300°. The Cm maximum was 0.4 at θ of 300°. In contrast, the minimum value of Cm appears at 0°, 120°, dan 360°. The Cm minimum was 0.015 at θ of 360°. As Song et al.[32] reported, the upwind region has a higher Cm value than the downwind region. As shown in Figure 12, the upwind region moment characteristics always show a positive Cm, while some downwind regions have a negative Cm. The moment characteristics depend on the wind velocity [35]. The Cm value constantly grew from θ of 35° until it reached the peak value at θ of 60°, then again decreased until θ of 120°. The trend was repeated for every θ of 120°. The obtained Cm value for one rotational period is then considered the Cm average to evaluate the Cp. The extracted Cm data from the simulation revealed that for each TSR value, the Cm average is 0.079, 0.152, 0.230, 0.172, dan 0.094, respectively, for TSR of 0.5, 1, 1.5, 2, and 2.5. The highest Cm falls at TSR 1.5.

The comparison of Cm value for rotor blades without and with VGs is depicted in Figures 13 and 14, respectively, for rectangular and triangular. Compared with the blade without VGs, the rectangular VGs show the highest increment at a TSR of 1.5. While the highest increment for triangular VGs found at the TSR value of 1. Figure 13 plots the polar chart for rectangular VGs at a TSR value of 1.5. As can be seen from Figure 13 that the use of VGs enhances the Cm value for each azimuth angle (θ). The highest Cm value was 0.443 at θ of 60°, x/c of 25 %, and TSR of 1.5. The trend of Cm for a blade with triangular VGs was similar to that of the blade without VGs. The maximum Cm value occurs when the turbine rotates at θ of 60°, 180°, dan 300°. In contrast, the minimum value of Cm appears at 0°, 120°, dan 240°. The minimum value of Cm was shifted to 120° as compared to the rotor blade without VGs. The presence of VGs also benefits by resulting in a positive Cm value for one cycle of the rotational turbine. The chordwise variation (x/c) shows a slightly different enhancement of the Cm compared to the rotor blade without VGs.

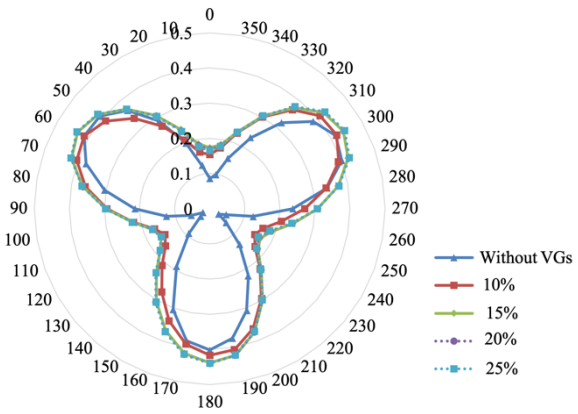

Fig. 13: Comparison of polar chart of Cm with respect to θ during one rotational period at TSR of 1.5 between rotor blade without VGs and rectangular VGs.

Figure 14 shows that triangular VGs would also improve the Cm values. The highest Cm value was 0.509 at x/c of 20 % and TSR of 1. In addition, the maximum Cm value occurs when the turbine rotates at θ of 80°, 200°, dan 320°. In comparison, the minimum value of Cm appears at 20°, 140°, dan 260°. The minimum value of Cm was shifted to 120° as compared to the rotor blade without VGs. In the triangular VGs, the variation of x/c shows a large difference in the curves, particularly in the upwind region. However, their total increment is still lower than

the rectangular VGs. The reason behind the trend might explain using flow field characteristics which will be provided hereafter.

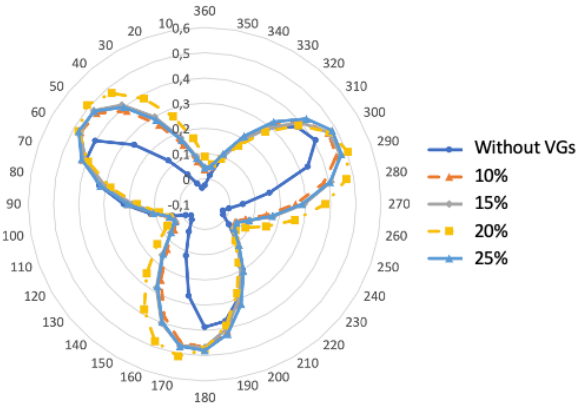

Fig. 14: Comparison of polar chart of Cm with respect to θ during one rotational period at TSR of 1 between rotor blade without VGs and triangular VGs.

3.2 The effect of Vortex Generators on Power Coefficient (Cp)

Figure 15 shows the power coefficient (Cp) variation of rotor blades without VGs and with rectangular VGs at x/c of 10%, 15%, 20%, and 25% towards the different tip speed ratios (TSR). For all the cases, the Cp value increased sharply until the TSR of 1.5, then decreased after that. The turbine generates less torque in high TSR, affecting the decrease of Cp. The comparison to rotor blades without VGs shows that the highest increment of Cp using the rectangular VGs was in the average of 47.24% for TSR of 1.5 and x/c of 25%. From Figure 15, it is interesting to notice at x/c of 10% and TSR of 2.5, the Cp of the blade without VGs was higher than that of the blade with VGs. At high TSR, the turbine angular velocity is also high, resulting in drag force enhancement. Though the lift coefficient increased simultaneously, the presence of VGs could not suppress the negative effect of the VGs. The rectangular VGs generate a high lift force followed by a high drag force [36].

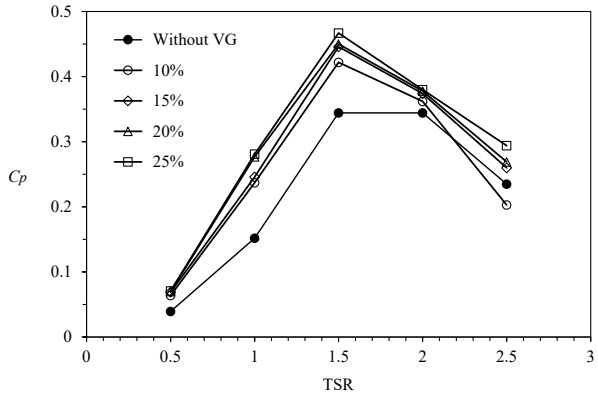

Fig. 15: The Cp value at different TSR for blade without VGs and with rectangular VGs.

As mentioned above, the best performance was at x/c of 25%, where VGs indicate that the lift could suppress the induced drag in this variation. The H-rotor wind turbine has a unique characteristic where the angle of attack constantly changes due to the rotation of the wind turbine on the vertical axis. This would be a challenge in developing a rotor blade that can delay the flow separation under a fluctuating angle of attack.

Figure 16 depicts the results of the power coefficient toward TSR variation for the blade without VGs and with triangular VGs under different x/c. As expected, the VGs would enhance the Cp compared to the blade without VGs. It is indicated from Figure 16 that each variation of the blade with triangular VGs has a higher value as compared to the blade without VGs.

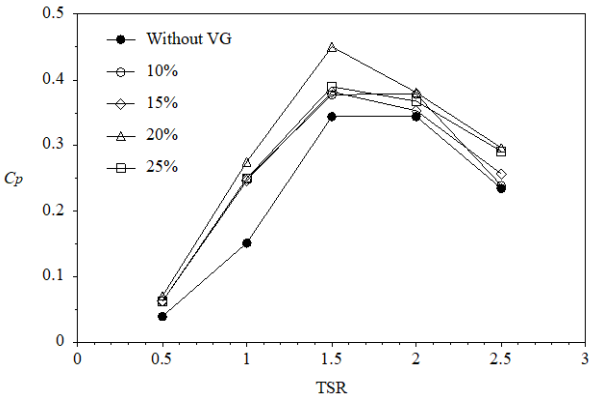

Fig. 16: The Cp value at different TSR for blade without VGs and with triangular VGs.

The VGs could enhance Cp by about 45.68% at x/c of 20% and TSR of 1.5. The peak value of Cp was in a TSR of 1.5, and then it gradually decreased when the TSR increased. However, the Cp value of VGs remains higher than without VGs. Slightly different from rectangular VGs, the best position of triangular VGs is in the x/c position of 20%, where the lift force is the highest. Figures 15 and 16 indicate that using VGs on the H-rotor airfoil could improve the Cp generated by the turbine. VGs create a vortex that transforms the laminar sublayer in the airfoil surface's boundary layer, accelerating the development of the turbulent flow. The transformation of laminar into turbulent flow effectively delays the flow separation leading to the delaying the stall while increasing the lift force. Hence the presence of VGs both for triangular and rectangular provides a significant effect on performance enhancement.

3.3 The effect of Vortex Generators on Vortex Development

The vortex development of the VGs is represented by the turbulent kinetic energy (TKE), as shown in Figure 17. Figure 17 shows the comparison of the TKE towards the chordwise (x/c) position for the blade without VGs and with rectangular and triangular VGs. As can be seen from

Figure 17, the TKE for the VGs much higher than the blade without VGs. In the blade without VGs, only small TKE energy was observed in the blade tip. However, the blade with rectangular and triangular VGs shows a high TKE towards the leading and trailing edges. The vortex generators create vortices in the boundary layer that are essentially parallel to the airflow direction over the blade. These vortices increase the TKE of the airflow closest to the blade's surface by moving faster air from the boundary layer's outer region down to the region near the surface, strengthening the boundary layer and delaying its separation. Wake region development on the blade with VGs also contributes to the higher value of TKE. Therefore, as the higher TKE appeared in the blade with VGs, their power coefficient tended to be higher than the blade without VGs.

At the chordwise position (x/c), the TKE shows the highest TKE at x/c of 25% for rectangular and 20% for triangular. For the VGs, the TKE improved with the increase of x/c until it reached the maximum and decreased. Since the post-stall behavior depends on the x/c position, it will be crucial to decide on the VGs position [37]. If the position is too far from the downstream, it will affect the sudden decrease of lift force. At x/c <20%, both VGs experienced a considerable lift force with less drag force. However, after x/c >20%, the drag force rose under the increase of the lift force. Therefore, it is suggested to have the VGs position at x/c ≤ 20% to maximize the power output. The position implies the best compromise between post-stall behavior and performance enhancement. The net of imbalance lift and drag force will decide the performance.

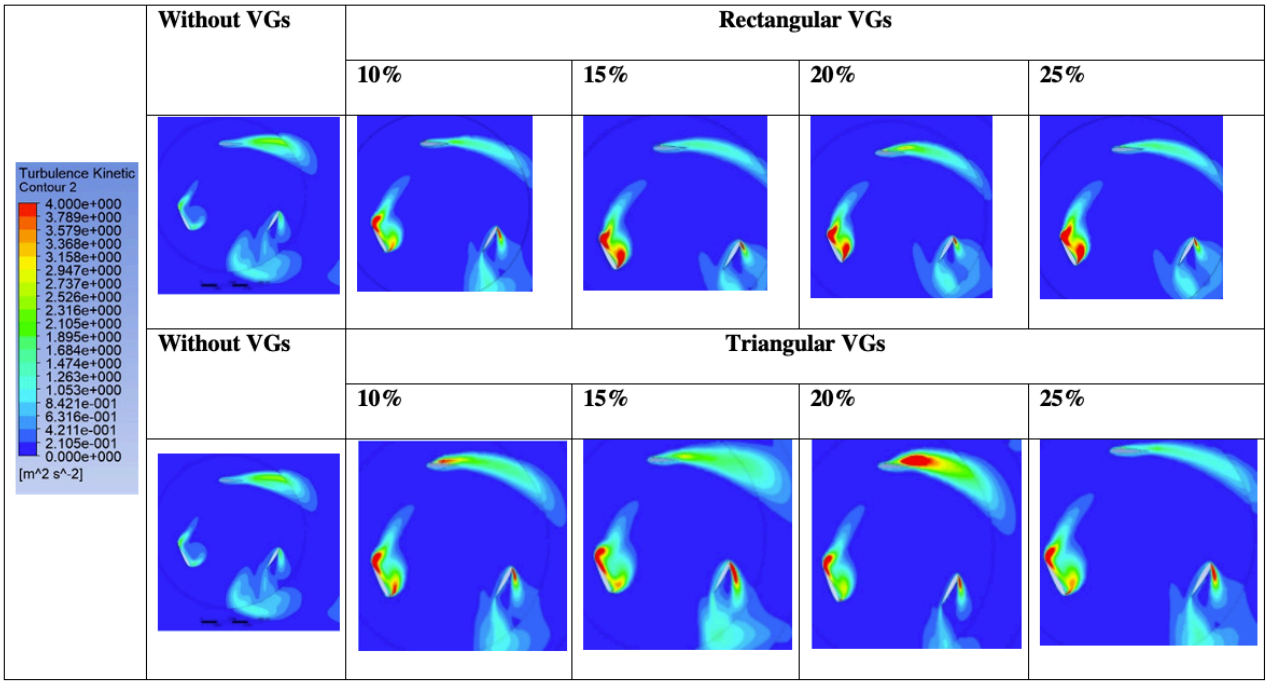

Fig. 17: Turbulent kinetics energy towards the chordwise (x/c) for blade with and without VGs.

3.4 The effect of Vortex Generators on Flow Field

Figure 18 compares the blade's flow field velocity without VGs and rectangular and triangular VGs towards the chordwise (x/c) variations. The fluid velocity around the blade surface can indicate how much the impact of the VGs and vortex their vortex development. The turbulent flow generated by the VGs improves the flow velocity in the impacted region, which would also delay the fluid separation in the airfoil.

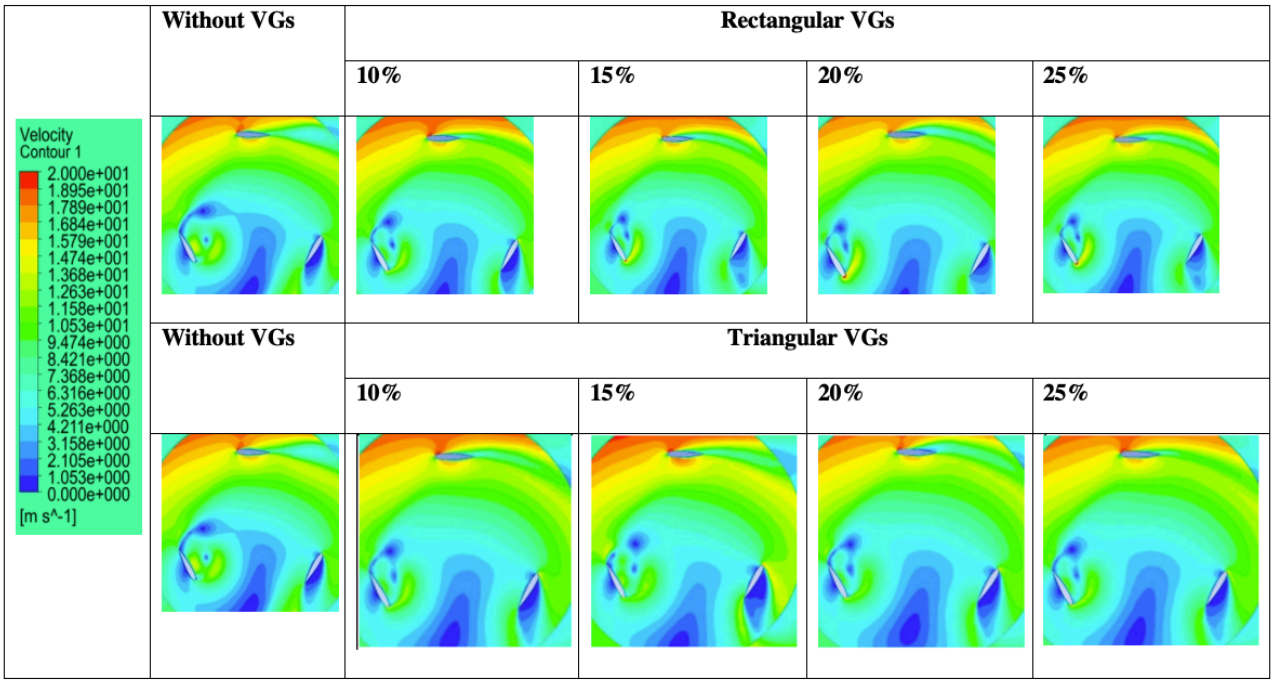

Fig. 18: Flow field velocity towards the chordwise (x/c) for blade with and without VGs.

As seen in Figure 18, the velocity of the turbine with VGs was higher than without VGs. It is consistent with the turbulent kinetic energy generation in Figure 17. The laminar boundary layer of the airfoil is gradually transformed into turbulent flow due to the presence of VGs, leading to a speedy velocity. Figure 18 shows fluid velocity improvement, especially at the suction and pressure sides of the blade with VGs. The fluid velocity improvement affects the lift force enhancement, which impacts the coefficient moment intensification.

4. Conclusions

The current study provides a numerical study on the effect of the vortex generators (VGs) on the H-rotor blade of a wind turbine using ANSYS FLUENT with URANS modeling. Two VGs in rectangular and triangular shapes were attached to the blade surface to improve the performance. To evaluate their performance, the rotor blade without VGs also was investigated in the current study. The effect of chordwise (x/c) was evaluated to suggest the best embodiment position of the VGs on the blade surface. According to the simulation results, we found that:

- The VGs improve the moment coefficient (Cm), and Power coefficient (Cp) compared to the rotor blade without VGs. The rectangular VGs show the highest increment at a TSR of 1.5. However, the highest increment for triangular VGs found at the TSR value of 1.
- For rectangular VGs, the highest Cm value was found at 0.443 at θ of 60°, x/c of 25 %, and TSR of 1.5. While for triangular VGs, the highest Cm value was found at 0.509 at x/c of 20 % and TSR of 1.
- In terms of Cp, the rectangular VGs had the maximum power coefficient (Cp) value at the x/c of 20%, while the triangular VGs had the maximum Cp value at the x/c of 25%. However, both VGs show the maximum Cp in the value of 0.467 with a 1.5 Tip Speed Ratio (TSR).
- The best position of x/c for the rectangular was at 25%, while the triangular was 20% as the best compromise between the performance enhancement and stall behavior.
- The performance improvement shows that the blade with VGs improves the performance of the wind turbine by around 45.68% and 47.24%, respectively, for triangular and rectangular.
- The turbulent kinetic energy (TKE) and velocity field revealed that the VGs could suppress the flow separation by generating vortex flow at the surface of the airfoil. They induce vortices at the boundary layer, leading to the increase of turbulent kinetic energy.

Acknowledgements

This research was fully supported by PNBP grant from the Universitas Sebelas Maret, Indonesia, with contract number 260/UN27.22/HK.07.00/2021 of the mandatory scheme.

References

1) P. Byrne, P. Nandy, M. Thierrry, and A. Nasruddin, Design of a Solar AC System Including a PCM Storage for Sustainable Resorts in Tropical Region, " *Evergreen*, 6 (2), 143-148, (2019). https://doi.org/10.5109/2321009.
2) L. K. Sagar, and D. B. Das, "Fuzzy Expert System for Determining State of Solar Photo Voltaic Power Plant Based on Real-Time Data," *Evergreen*, 9 (3), 870-880, (2022). https://doi.org/10.5109/4843118.
3) O. Choupin, A. Têtu, B. Del Río-Gamero, F. Ferri, and JP. Kofoed, "Premises for an annual energy production and capacity factor improvement towards a few optimised wave energy converters configurations and resources pairs," *Applied Energy*, 312, 118716, ISSN 0306-2619, (2022). https://doi.org/10.1016/j.apenergy.2022.118716.
4) I. Collins, M. Hossain, W.Dettmer, and I. Masters, "Flexible membrane structures for wave energy harvesting: A review of the developments, materials and computational modelling approaches," *Renewable and Sustainable Energy Reviews*, 151, 111478, ISSN 1364-0321, (2021). https://doi.org/10.1016/j.rser.2021.111478.
5) G. Yohanes, P. Nandy, K. Eny, and I. I. Hakim, "Study of Heat Pipe Utilizing Low-Temperature Geothermal Energy and Zeolite-A for Tea Leaves Withering Process," *Evergreen*, 7 (2), 221-227, (2020). https://doi.org/10.5109/4055223.
6) B. T., Prasetyo, Suyanto, MAM. Oktaufik and S. Hakim, "Design, Construction and Preliminary Test Operation of BPPT-3MW Condensing Turbine Geothermal Power Plant," *Evergreen*, 6 (2), 162-167, (2019). https://doi.org/10.5109/4055223.
7) R. Alipour, R. Alipour, F. Fardian, and M. Hossein Tahan, "Optimum performance of a horizontal axis tidal current turbine: A numerical parametric study and experimental validation," Energy Conversion and Management, 258, 115533, ISSN 0196-8904, (2022). https://doi.org/10.1016/j.enconman.2022.115533.
8) N. Rodrigues, P. Pintassilgo, F. Calhau, E. González-Gorbeña, and A. Pacheco, "Cost-benefit analysis of tidal energy production in a coastal lagoon: The case of Ria Formosa – Portugal," Energy, 229, 120812, ISSN 0360-5442, (2021). https://doi.org/10.1016/j.energy.2021.120812.
9) M. Al-Ghriybah, "Performance Analysis of a Modified Savonius Rotor Using a Variable Blade Thickness," *Evergreen*, 9 (3), 645-653, (2022). https://doi.org/10.5109/4842522.
10) D. D. D. P. Tjahjana, I. Yaningsih, B. Y. L. Imama, and A. R. Prabowo "Aerodynamics Performance Enhancement of Wing Body Micro UAV Employing Blended Winglet Configuration," *Evergreen*, 8 (4), 799-811, (2021). https://doi.org/10.5109/4742122.
11) V. Kouloumpis, and A. Azapagic, "A model for estimating life cycle environmental impacts of offshore wind electricity considering specific characteristics of wind farms," Sustainable Production and Consumption, 29, 495-506, ISSN 2352-5509, (2022). https://doi.org/10.1016/j.spc.2021.10.024.
12) I. Marinić-Kragić, D. Vučina, and Z. Milas, "Robust optimization of Savonius-type wind turbine deflector blades considering wind direction sensitivity and production material decrease," Renewable Energy, 192, 150-163, ISSN 0960-1481, (2022). https://doi.org/10.1016/j.renene.2022.04.118.
13) I.Marinić-Kragić, D. Vučina, and Z. Milas, "Global optimization of Savonius-type vertical axis wind turbine with multiple circular-arc blades using validated 3D CFD model," Energy, 241, 122841, ISSN 0360-5442, (2022). https://doi.org/10.1016/j.energy.2021.122841.
14) Y. Ma, C. Chen, T. Fan, H. Lu, and J. Fang, "An innovative aerodynamic design methodology of wind turbine blade models for wind tunnel real-time hybrid tests based on genetic algorithm," Ocean Engineering, 257, 111724, ISSN 0029-8018, (2022). https://doi.org/10.1016/j.oceaneng.2022.111724.
15) H.A. Porto, C.A. Fortulan, and A.J.V. Porto, "Power performance of starting-improved and multi-bladed horizontal-axis small wind turbines," Sustainable Energy Technologies and Assessments, 53, Part A, 102341, ISSN 2213-1388, (2022). https://doi.org/10.1016/j.seta.2022.102341.
16) Z. Wang, and M. Zhuang, "Leading-edge serrations for performance improvement on a vertical-axis wind turbine at low tip-speed-ratios," Applied Energy, 208, 1184-1197, ISSN 0306-2619, (2017). https://doi.org/10.1016/j.apenergy.2017.09.034.
17) S. Sridhar, J. Joseph, and J. Radhakrishnan, "Implementation of tubercles on Vertical Axis Wind Turbines (VAWTs): An Aerodynamic Perspective," Sustainable Energy Technologies and Assessments, 52, Part B, 102109, ISSN 2213-1388, (2022). https://doi.org/10.1016/j.seta.2022.102109.
18) Z. Wang, A. Ozbay, W. Tian, and H. Hu, "An experimental study on the aerodynamic performances and wake characteristics of an innovative dual-rotor wind turbine," Energy, 147, 94-109, ISSN 0360-5442, (2018). https://doi.org/10.1016/j.energy.2018.01.020.
19) J. Thé, and H. Yu, "A critical review on the simulations of wind turbine aerodynamics focusing on hybrid RANS-LES methods," Energy, 138, 257-289, ISSN 0360-5442, (2017). https://doi.org/10.1016/j.energy.2017.07.028.

20) J. Zhong, J. Li, P. Guo, and Y. Wang, "Dynamic stall control on a vertical axis wind turbine aerofoil using leading-edge rod," Energy, 174, 246-260, ISSN 0360-5442, (2019). https://doi.org/10.1016/j.energy.2019.02.176.
21) R. Jiang, Z. Zhao, H. Liu, T. Wang, M. Chen, J. Feng, and D. Wang, "Numerical study on the influence of vortex generators on wind turbine aerodynamic performance considering rotational effect," Renewable Energy, 186, 730-741, ISSN 0960-1481, (2022). https://doi.org/10.1016/j.renene.2022.01.026.
22) C. Zhu, Y. Qiu, Y. Feng, T. Wang, and H. Li, "Combined effect of passive vortex generators and leading-edge roughness on dynamic stall of the wind turbine airfoil," Energy Conversion and Management, 251, 115015, ISSN 0196-8904, (2022), https://doi.org/10.1016/j.enconman.2021.115015.
23) R. Mereu, S. Passoni, and F. Inzoli, "Scale-resolving CFD modeling of a thick wind turbine airfoil with application of vortex generators: Validation and sensitivity analyses," Energy, 187, 115969, ISSN 0360-5442, (2019), https://doi.org/10.1016/j.energy.2019.115969.
24) D. D. Tavernier, C. Ferreira, A. Viré, B. LeBlanc, and S. Bernardy, "Controlling dynamic stall using vortex generators on a wind turbine airfoil," Renewable Energy, 172, 1194-1211, ISSN 0960-1481, (2021) https://doi.org/10.1016/j.renene.2021.03.019.
25) C. Zhu, J. Chen, Y. Qiu, and T. Wang, "Numerical investigation into rotational augmentation with passive vortex generators on the NREL Phase VI blade," Energy, 223, 120089, ISSN 0360-5442, (2021). https://doi.org/10.1016/j.energy.2021.120089.
26) L. Zhang, X. Li, K. Yang, and D. Xue, "Effects of vortex generators on aerodynamic performance of thick wind turbine airfoils," Journal of Wind Engineering and Industrial Aerodynamics, 156, 84-92, ISSN 0167-6105, (2016) https://doi.org/10.1016/j.jweia.2016.07.013.
27) D. Lengani, D. Simoni, M. Ubaldi, P. Zunino, and F. Bertini, "Turbulent boundary layer separation control and loss evaluation of low profile vortex generators," Experimental Thermal and Fluid Science, 35 (8), 1505-1513, ISSN 0894-1777, (2011). https://doi.org/10.1016/j.expthermflusci.2011.06.011.
28) Z. Zhao, R. Jiang, J. Feng, H. Liu, T. Wang, W. Shen, M. Chen, D. Wang, and Y.Liu, "Researches on vortex generators applied to wind turbines: A review," Ocean Engineering, 253, 111266, ISSN 0029-8018, (2022). https://doi.org/10.1016/j.oceaneng.2022.111266.
29) J. T. Hansen, M. Mahak, and I. Tzanakis, "Numerical modelling and optimization of vertical axis wind turbine pairs: A scale up approach," Renewable Energy, 171, 1371-1381, ISSN 0960-1481, (2021). https://doi.org/10.1016/j.renene.2021.03.001.
30) C. Zhu, J. Chen, J. Wu, and T. Wang, "Dynamic stall control of the wind turbine airfoil via single-row and double-row passive vortex generators," Energy, 189, 116272, ISSN 0360-5442, (2019) https://doi.org/10.1016/j.energy.2019.116272.
31) M.H. Mohamed, A. Dessoky, and F. Alqurashi, "Blade shape effect on the behavior of the H-rotor Darrieus wind turbine: Performance investigation and force analysis," Energy, 179, 1217-1234, ISSN 0360-5442, (2019). https://doi.org/10.1016/j.energy.2019.05.069.
32) C. Song, G. Wu, W. Zhu, X. Zhang, and J. Zhao, "Numerical Investigation on the Effects of Airfoil Leading Edge Radius on the Aerodynamic Performance of H-Rotor Darrieus Vertical Axis Wind Turbine," Energies., 12(19):3794 , (2019). https://doi.org/10.3390/en12193794.
33) C. Song, Y. Zheng, Z. Zhao, Y. Zhang, C. Li, H. Jiang, "Invetigation of meshing stategies and turbulence models of CFD simulations of vertical axis wind turbine," Journal of Renewable and Sustainable Energy, 7, 033111- 1 -19, (2025). http://dx.doi.org/10.1063/1.4921578.
34) ANSYS, ANSYS FLUENT 12.0 User's Guide, Release 12.0, ANSYS, Inc, 2009.
35) T. Pujol, A. Massaguer , E. Massaguer, L. Montoro and M. Comamala, "Net Power Coefficient of Vertical and Horizontal Wind Turbines with Crossflow Runners," Energies, 11(110), (2018). doi:10.3390/en11010110.
36) Y. Yan, E. Avital, J. Williams, J. Cui, "CFD analysis for the performance of micro-vortex generator on aerofoil and vertical axis turbine," Journal of Renewable and Sustainable Energy. 11, 043302 (2019). https://doi.org/10.1063/1,5110422.
37) H. Mueller-Vahl, G. Pechlivanoglou, CN. Nayeri, and C.O, Paschereit, "Vortex Generators for Wind Turbine Blades: A Combined Wind Tunnel and Wind Turbine Parametric Study." Proceedings of the ASME Turbo Expo 2012: Turbine Technical Conference and Exposition. Volume 6: Oil and Gas Applications; Concentrating Solar Power Plants; Steam Turbines; Wind Energy. Copenhagen, Denmark. June 11–15, 899-914 (2012) . https://doi.org/10.1115/GT2012-69197.